




Effect of heterogeneous environmental conditions on labyrinthine vegetation patternsS. Echeverría-Alar ¹, D. Pinto-Ramos ¹, M. Tlidi,² and M. G. Clerc ¹¹*Departamento de Física and Millennium Institute for Research in Optics, FCFM, Universidad de Chile, Casilla 487-3, Santiago, Chile*²*Faculté des Sciences, Université libre de Bruxelles (U.L.B), CP 231, 1050 Brussels, Belgium*

(Received 31 August 2022; revised 4 April 2023; accepted 24 April 2023; published 23 May 2023)

Self-organization is a ubiquitous phenomenon in Nature due to the permanent balance between injection and dissipation of energy. The wavelength selection process is the main issue of pattern formation. Stripe, hexagon, square, and labyrinthine patterns are observed in homogeneous conditions. In systems with heterogeneous conditions, a single wavelength is not the rule. Large-scale self-organization of vegetation in arid environments can be affected by heterogeneities, such as interannual precipitation fluctuations, fire occurrences, topographic variations, grazing, soil depth distribution, and soil-moisture islands. Here, we investigate theoretically the emergence and persistence of vegetation labyrinthine patterns in ecosystems under deterministic heterogeneous conditions. Based on a simple local vegetation model with a space-varying parameter, we show evidence of perfect and imperfect labyrinthine patterns, as well as disordered vegetation self-organization. The intensity level and the correlation of the heterogeneities control the regularity of the labyrinthine self-organization. The phase diagram and the transitions of the labyrinthine morphologies are described with the aid of their global spatial features. We also investigate the local spatial structure of labyrinths. Our theoretical findings qualitatively agree with satellite images data of arid ecosystems that show labyrinthinelike textures without a single wavelength.

DOI: [10.1103/PhysRevE.107.054219](https://doi.org/10.1103/PhysRevE.107.054219)**I. INTRODUCTION**

Self-organization is a universal feature of out-of-equilibrium systems and is of common occurrence in many fields of nonlinear science [1–4]. The spontaneous emergence of self-organized dissipative structures out of a homogeneous state has been observed in many out-of-equilibrium systems, including biology, chemical reaction-diffusion systems, fluid mechanics, nonlinear optics, and laser physics [1–3]. On the one hand, these systems are subjected to a balance between a nonlinear effect and a transport or a spatial coupling process. On the other hand, they are subjected to a continuous injection and dissipation of energy. The balance between these processes triggers the emergence of dissipative structures with an intrinsic macroscopic scale [2,5,6], which corresponds to a spontaneous symmetry-breaking instability. Over the past decades, extensive research has been done to understand the origins of simple patterns, such as stripes, hexagons, and squares, from a theoretical point of view [2,7]. However, nontrivial symmetry patterns, i.e., labyrinths, have gotten little attention due to their complicated structure, rich in spatial defects [8,9]. Recently, an attempt to characterize this ubiquitous phenomenon has introduced a quantitative definition of *ideal* labyrinthine patterns [10], which satisfy the following: (i) the disordered patterns are characterized globally by a powdered ring Fourier spectrum, and (ii) the spatial structures are described locally by a single wave mode. The *ideal* adjective refers to labyrinths with a single dominant characteristic wavelength, which are observed in controlled physical contexts, e.g., ferrofluids, chemical reactions, cholesteric liquid crystals, block copolymers, metal nanosurfaces, and ferroelectric thin films [11–16].

Self-organized structures arise in plant ecology, where stressed vegetation biomass can self-organize when resources, such as water or nutrients, are limited [17–24]. Under these arid conditions, the plant community displays coherent distributions, which are maintained by facilitative and competitive processes involving plants and the environment [18]. These distributions, whose wavelengths range from centimeter to kilometer scales, are frequently referred to as vegetation patterns. Starting from a uniform cover, as the aridity level is increased, the first pattern that appears consists of a periodic spatial distribution of gaps followed by labyrinths and then spots. This generic sequence has been predicted using various pattern-forming ecological models. The first paper that discusses the sequence was [19] in 1999. Later on, the sequence was analyzed from reaction-diffusion models in 2001 [20] and 2002 [21]. The sequence gaps-stripes/labyrinths-spots as a function of the aridity has been empirically studied in an arid region of Sudan [24]. There, the term labyrinth was used to describe disordered vegetation bands in a flat surface [20–25]. Besides periodic, other aperiodic and localized vegetation patterns have been reported [26–31]. Well-documented localized vegetation patterns are the fairy circles [32–39]. Localized vegetation patterns can exhibit curvature instabilities leading either to the self-replication phenomenon [40,41], or the formation of arcs and spirals [42]. Other alternative hypotheses for the spatial structure of vegetation self-organization have been explored, such as random patterns and power-law distributions of patch sizes [43,44].

In ecological systems, the presence of spatial and/or temporal heterogeneities may influence the self-organization of plant communities. The causes of heterogeneities are frequently related to variations in interannual precipitation,

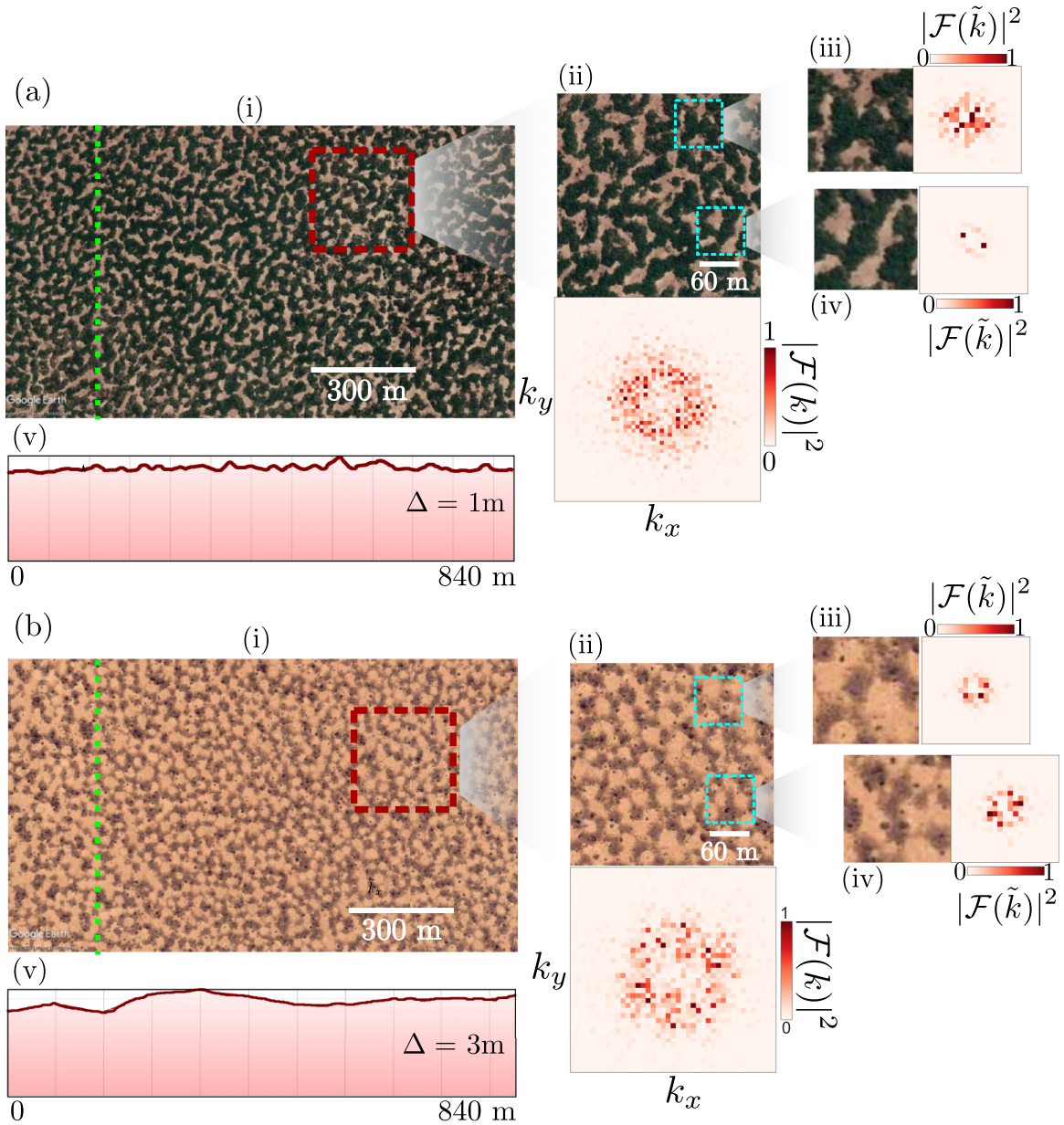


FIG. 1. Satellite images of vegetation labyrinths. Self-organization of vegetation observed in (a)(i) Niger ($12^{\circ}27'50.58''$ N $3^{\circ}18'30.76''$ E) and (b)(i) Sudan ($11^{\circ}18'26.07''$ N $27^{\circ}57'58.62''$ E). The (ii) insets display a zoom of images in (i) and are characterized by their Fourier transform $|\mathcal{F}(k)|^2$. The (iii) and (iv) insets are local regions of the images in (ii) accompanied by their local Fourier transforms $|\mathcal{F}(\tilde{k})|^2$. The (v) insets correspond to elevation profiles along the green dotted lines in (i). The value of Δ indicates the difference between the maximum and the minimum height. The vegetation snapshots and elevation profiles were retrieved from Google Earth Pro software.

occurrences of fire, topographic changes, grazing, soil depth distribution, and soil-moisture islands [22,45–49]. It makes sense to infer that one or more of the aforementioned heterogeneities control the irregularities in vegetation patterns (see the labyrinthinelike structures in Fig. 1). In the majority of the ecological mathematical models, these heterogeneous effects are not included, resulting in far too ideal vegetation patterns, or are approached by stochastic processes in time [46,47,49,50] or space [51]. To our knowledge, the role of deterministic heterogeneities in forming different labyrinthinelike vegetation patterns and controlling their possible transitions has not been addressed. Understanding the conditions under which heterogeneous labyrinths arise is

relevant from an ecological perspective as it sheds light on the self-organization of vegetation in isotropic real ecosystems (Fig. 1). Furthermore, the study of these types of vegetation self-organization can contribute to the discussion on how heterogeneities in arid or semiarid systems can avoid catastrophic shifts [27,51,52], which corresponds to abrupt transitions between a vegetated cover and bare soil, by establishing irregular vegetation mosaics.

In this article, we investigate theoretically the role of deterministic heterogeneities in shaping labyrinthinelike vegetation patterns as equilibria in arid and semiarid landscapes. For this purpose, we use a well-established model for vegetation biomass, where the effects of heterogeneities are modeled

as spatial variations around a mean aridity parameter. The heterogeneities are controlled by their intensity and degree of correlation. Different equilibria are numerically observed after the temporal evolution of the biomass. These vegetation patterns are characterized by their structure factor and their spatial Fourier transform at a global and local scale. These tools allow us to differentiate between perfect and imperfect labyrinths, and disordered self-organization. We construct a phase diagram and show that a minimum intensity level and/or degree of correlation are needed to observe imperfect labyrinthine patterns. This equilibrium qualitatively resembles the labyrinthine-like patterns observed in nature (Fig. 1). Finally, we discuss a possible implementation of our classification in natural landscapes.

II. LABYRINTHINE-LIKE PATTERNS IN ECOSYSTEMS

It is crucial to identify whether plants have structures resembling labyrinths to assess if they fulfill the definition of a labyrinth proposed recently [10]. Figures 1(a i) and 1(b i) show two examples of labyrinthine-like self-organized structures in Niger and Sudan, respectively. These vegetation images can be characterized by their Fourier spectrum at different scales as shown in insets (ii), (iii), and (iv) of Fig. 1. The insets (ii) exhibit the disordered feature of the self-organization at a global scale. The Fourier transform is nearly isotropic and highly scattered, involving several wave vectors (powderlike ring spectrum). The insets (iii) and (iv) of Fig. 1 show the spatial behavior at a local scale. The local Fourier transforms do not show a dominant single wave vector pair structure. Specifically, two diametrically opposed peaks are not visible in the local two-dimensional Fourier transform, and more complex structures are exhibited. As a result, neither the landscapes of Niger nor of Sudan meet the criteria for a perfect labyrinthine pattern [10]. We attribute the departure from the ideal pattern to the presence of heterogeneities in the regions shown in Fig. 1. The insets (v) in Figs. 1(a) and 1(b) display the topographic variations of the terrain in Niger and Sudan, respectively. Indeed, the topography is a source of spatial heterogeneity for the vegetation local self-organization [53–55]. In the following, we suppose that these topographic fluctuations affect the resource distribution on the Niger and Sudan landscapes.

III. THEORETICAL MODELING APPROACH

We choose to model the emergence of vegetation patterns from the perspective of symmetry-breaking instabilities of homogeneous covers in arid or semiarid environments [18]. Particularly, we use an interaction-redistribution approach for plant community behavior, where the biomass density $c = c(\mathbf{r}, t)$ at space point $\mathbf{r} = (x, y)$ and time t evolves following a logistic equation that includes nonlocal interactions of the biomass [33]:

$$\partial_t c = c(1 - c)M_f(\mathbf{r}) - \mu c M_c(\mathbf{r}) + D M_d(\mathbf{r}). \quad (1)$$

The first term on the right-hand side (rhs) of Eq. (1) models the rate at which biomass increases and eventually saturates. The nonlocal function $M_f(\mathbf{r}) = \exp[\chi_f \int d\mathbf{r}' \phi_f(\mathbf{r}', L_f) c(\mathbf{r} + \mathbf{r}')]]$ accounts for interactions facilitating growth, regulated by

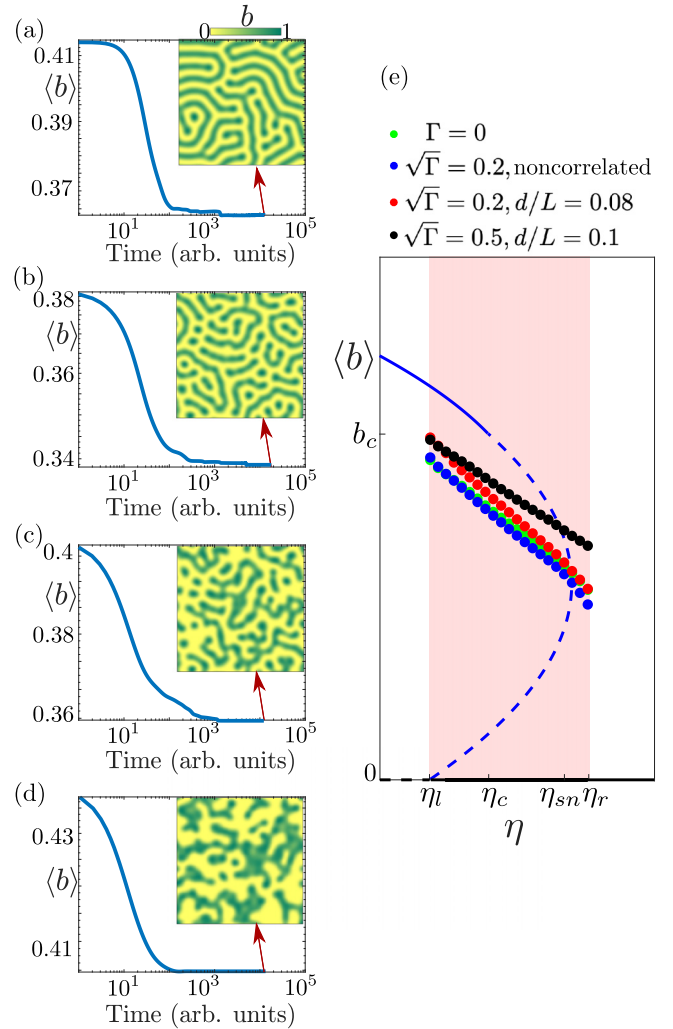


FIG. 2. Equilibrium patterns of Eq. (2) in a square domain of size $L = 240$ (arb. units) with $\kappa = 0.6$, $\nu = 0.011$, $\gamma = 0.5$, and $\alpha = 0.125$. The temporal evolutions of the spatially averaged biomass $\langle b \rangle$ are displayed for the (a) homogeneous case $\Gamma = 0$, and the inhomogeneous cases $\Gamma \neq 0$ considering both (b) noncorrelated and (c),(d) correlated heterogeneities. The insets show the respective equilibria. (e) Bifurcation diagram of Eq. (2). The black lines correspond to the bare state and the blue curves account for the uniform vegetated state in the homogeneous case $\Gamma = 0$. The continuous (broken) lines indicate that these analytical solutions are stable (unstable). In the shaded region, limited by η_l and η_r , the labyrinthine patterns in homogeneous conditions are stable. In this subfigure, $\langle b \rangle$ is the mean value over 30 random initial conditions around b_+ .

an intensity χ_f . These effects are controlled by the kernel function ϕ_f , whose range of influence is of the order of the plant's aerial structure L_f . The second term on the rhs of Eq. (1) represents the biomass death processes. $M_c(\mathbf{r}) = \exp[\chi_c \int d\mathbf{r}' \phi_c(\mathbf{r}', L_c) c(\mathbf{r} + \mathbf{r}')]]$ accounts for interactions enhancing biomass decay with an intensity χ_c . The parameter μ is a measure of the mortality-to-growth rate ratio of plants in the absence of interaction with others, which can be seen as resource scarcity or aridity [18,56]. This negative feedback acts over distances of the order of the root length L_c with an intensity χ_c and is controlled by the kernel function

ϕ_c . A cooperative measure of the ecological system can be introduced as $\chi_f - \chi_c$. The last term in Eq. (1) incorporates seeds dispersion with a diffusion parameter D , where $M_d(\mathbf{r}) = \int d\mathbf{r}' \phi_d(\mathbf{r}') [c(\mathbf{r} + \mathbf{r}') - c(\mathbf{r})]$, and $\phi_d(\mathbf{r}')$ accounts for the biomass transport between positions \mathbf{r} and \mathbf{r}' .

The integrodifferential equation (1), close to the double limit of nascent bistability (between uniform vegetation cover and bare soil) and the symmetry-breaking instability of the uniform cover, can be reduced to a partial differential equation. The reduced model reads [19,33]

$$\partial_t b = -\eta b + \kappa b^2 - b^3 + (v - \gamma b) \nabla^2 b - \alpha b \nabla^4 b, \quad (2)$$

where $b = b(\mathbf{r}, t)$ is the state variable associated to the biomass density close to nascent bistability. The parameters η and κ are the deviations of the aridity and cooperativity critical parameters, respectively. v and γ are linear and nonlinear diffusion coefficients, respectively. The last term is a nonlinear hyperdiffusion controlled by α . The parameters $\{v, \gamma, \alpha\}$ depend on the strength of the competitive feedback, the seed's diffusion, and the shape of the kernels ϕ_f , ϕ_c , and ϕ_d [30]. The model equation (2) has three homogeneous states: the bare state $b = 0$ [black line in Fig. 2(d)] and $b_{\pm} = (\kappa \pm \sqrt{\kappa^2 - 4\eta})/2$ [blue line in Fig. 2(d)]. The b_{\pm} equilibria are connected by a saddle-node bifurcation at $\eta_{\text{sn}} = \kappa^2/4$ with κ positive. The uniform solution b_- is always unstable. For small aridity, the vegetated state b_+ is stable. When the aridity is increased the uniform cover suffers a spatial instability. This spatial instability with critical wavelength $\lambda_c = 2\pi \sqrt{2\alpha/(\gamma - v/b_c)}$ occurs at $\eta \equiv \eta_c$, where η_c satisfies the implicit condition $4\alpha b_c^2(2b_c - \kappa) = (\gamma b_c - v)^2$ with $b_c \equiv b_+(\eta_c)$. Hence, the homogeneous cover b_+ is unstable to patterns within the range $\eta_c \leq \eta \leq \eta_{\text{sn}}$ [see Fig. 2(d)]. By fixing the parameters $\{\kappa, v, \gamma, \alpha\}$ in Eq. (2), labyrinthine patterns are stable within the aridity range $[\eta_l, \eta_r]$ as shown in Fig. 2(d).

To model the effect of heterogeneities in the labyrinths of Eq. (2), in principle, we must promote all parameters to be spatially dependent; that is, one should consider five functions $[\eta(\mathbf{r}), \kappa(\mathbf{r}), \alpha(\mathbf{r}), v(\mathbf{r}), \gamma(\mathbf{r})]$, which makes the theoretical and numerical studies cumbersome. To shed light on the effect of heterogeneities in the labyrinthine patterns, we promote the aridity parameter to be spatially dependent $\eta(\mathbf{r})$ and keep the other parameters homogeneous. Hence, in the following analysis, we focus on the model equation (2) with heterogeneous aridity $\eta(\mathbf{r}) = \eta + \sqrt{\Gamma} \xi(\mathbf{r})$, where η accounts for the mean aridity. This average value is inside the aridity range $[\eta_l, \eta_r]$. $\xi(\mathbf{r})$ models the spatial variations with zero mean value $\langle \xi(\mathbf{r}) \rangle = 0$ and intensity level Γ . The heterogeneities $\xi(\mathbf{r})$ can be spatially independent (delta correlated) or correlated. To obtain a spatially correlated function $\xi(\mathbf{r})$ characterized by a correlation length d , we consider a relaxation diffusive process with a random initial condition, which evolves until a given time [57]. Note that the results presented below are qualitatively similar if all parameters are spatially dependent.

IV. RESULTS

Let us introduce the spatially averaged biomass $\langle b \rangle \equiv \int_0^L \int_0^L b(\mathbf{r}, t) dx dy / L^2$, where L^2 is the system size. The charts

in the left panel of Fig. 2 show the temporal evolution to equilibrium for $\langle b \rangle$ according to Eq. (2) starting from the vegetated state b_+ in the symmetry-breaking regime $\eta_c \leq \eta \leq \eta_{\text{sn}}$. Figure 2(a) corresponds to the homogeneous case, $\Gamma = 0$, exhibiting an ideal labyrinthine pattern. Figure 2(b) represents the noncorrelated spatial variations, while Figs. 2(c) and 2(d) show the spatially correlated cases. In these cases, the striped structure of the labyrinthine pattern becomes locally distorted. Figure 2(e) shows the bifurcation diagram of Eq. (2). The labyrinthine-like patterns (dotted plots) are characterized by their averaged biomass $\langle b \rangle$. The green dotted curve indicates a branch of an ideal labyrinthine pattern when $\Gamma = 0$, which is stable in the range $\eta_l \leq \eta \leq \eta_r$. By increasing the aridity level, the labyrinth exhibits a transition to a mosaic of localized spots at $\eta > \eta_r$. When decreasing the aridity parameter, the labyrinthine pattern becomes clusters of hexagonal gaps at $\eta < \eta_l$ [31]. The blue dotted curve represents the stable branch of a vegetation pattern when $\Gamma \neq 0$ and ξ is noncorrelated. The red and black dotted curves are the stable branches of labyrinthine-like patterns under correlated heterogeneous conditions. We note that the impact of heterogeneities in the averaged biomass is not always strong [see red and blue dots in Fig. 2(e)]. Thus, other types of spatial tools are needed to understand and differentiate the labyrinthine-like equilibria of Eq. (2).

To characterize labyrinthine equilibria under homogeneous ($\Gamma = 0$) and heterogeneous ($\Gamma \neq 0$) conditions, we consider first the aridity distributions depicted in Fig. 3, and next we concentrate on the biomass densities $b_{\text{eq}}(\mathbf{r})$ shown in Fig. 4. We analyze the spatial structure of these aridities and biomass equilibria employing the Fourier transform amplitude $|\mathcal{F}(\mathbf{k})|^2 = |\int g(\mathbf{r}) e^{i\mathbf{k}\cdot\mathbf{r}} dx dy|^2$ and the structure factor $S(k) = \int_{-\pi}^{\pi} |\mathcal{F}(\mathbf{k})| k d\theta$, where $\mathbf{k} = (k \cos \theta, k \sin \theta)$, and $g(\mathbf{r})$ can be either $b_{\text{eq}}(\mathbf{r})$ or $\eta(\mathbf{r})$. The homogeneous and noncorrelated heterogeneous aridity distributions are characterized by a delta and a noisy flat $|\mathcal{F}(\mathbf{k})|^2$, respectively [see Figs. 3(a) and 3(b)]. The spatially correlated aridities have a nontrivial $S(k)$ shape associated with their coherent distribution [cf. Figs. 3(c) and 3(d)].

Let us now have a look at the biomass densities $b_{\text{eq}}(\mathbf{r})$ displayed in the top panels of Fig. 4. These equilibria are obtained by numerical simulations of the model equation (2) in square boxes. The spatial profiles of the aridity $\eta(\mathbf{r})$ used in these numerical simulations are the same as those in Fig. 3. Under homogeneous conditions, the biomass density exhibits a *perfect* labyrinthine pattern. The corresponding spectrum and the structure factor are shown in Fig. 4(a). From this figure, we see that the spectrum has a powdered ringlike shape and the structure factor presents a well-defined peak at $k = k_c$ [see Fig. 4(a)]. The finite width in the structure factor is attributed to the defects size and local variations of the wavevector [9]. The powdered ringlike shape indicates no preferred direction since the system is isotropic in the (x, y) plane. The full width at half maximum of $S(k)$ for the labyrinth in Fig. 4(a) is $w \approx 0.15k_c$. It is obtained by fitting a Lorentzian squared curve to the structure factor [58,59]. We define $w_h = k_c \pm w/2$ as the characteristic wavevector range of the perfect labyrinthine pattern, which emerges from a symmetry-breaking instability in Eq. (2). Figure 4(b) shows an equilibrium in the case of $\Gamma \neq 0$ and delta-correlated $\xi(\mathbf{r})$.

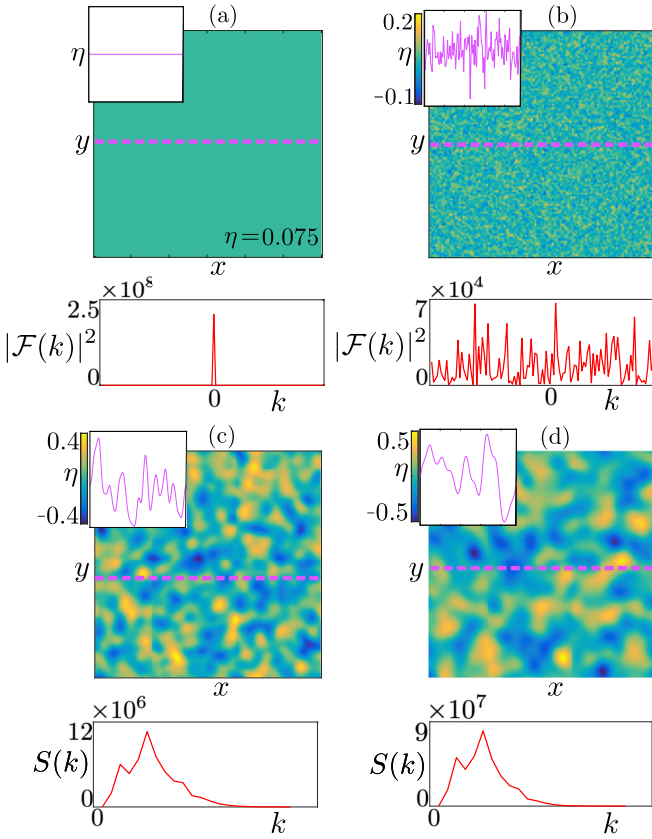


FIG. 3. Spatial distributions of the aridity parameters $\eta(\mathbf{r}) = \eta + \sqrt{\Gamma}\xi(\mathbf{r})$ with $\eta = 0.075$. In the top panels, the aridity distributions are shown. The insets correspond to an arbitrary one-directional cut represented by dashed pink lines. The lower panels illustrate the spatial structure of the distributions by their Fourier transform amplitude $|\mathcal{F}(\mathbf{k})|^2$ or structure factor $S(k)$. Other parameters are (a) $\Gamma = 0$; (b) $\sqrt{\Gamma} = 0.2$, $d/L = 0$; (c) $\sqrt{\Gamma} = 0.2$, $d/L = 0.08$; and (d) $\sqrt{\Gamma} = 0.5$, $d/L = 0.1$.

In this case, the labyrinth does not exhibit long fingers as in the homogeneous case due to the proliferation of local spots. Indeed, the heterogeneities introduce local disturbances in the wavevector reflected in the widening of $S(k)$ [cf. blue curve and inset in the bottom panel of Fig. 4(b)]. When the heterogeneities are sufficiently intense ($\sqrt{\Gamma} = 0.2$) and correlated ($d/L = 0.08$), the perfect labyrinthine pattern loses its structure and blobs of vegetation or bare soil emerge [see Fig. 4(c)]. In this aridity level, the maximum of the structure factor \hat{k} lies outside w_h [cf. blue curve in the bottom panel of Fig. 4(c)]. We define this shift in \hat{k} as a transition from perfect labyrinths ($|\hat{k} - k_c| < w_h$) to *imperfect labyrinthine patterns* ($|\hat{k} - k_c| > w_h$). When further increasing the correlation and the intensity level of the heterogeneities ($\sqrt{\Gamma} = 0.5$ and $d/L = 0.1$), the labyrinthine pattern is almost completely lost. A few vegetated fingers coexist with homogeneous islands of vegetation and bare soil [see the top panel in Fig. 4(d)]. As seen in the bottom panel of Fig. 4(d), the peak of the structure factor exhibits a significant shift (from $\hat{k} = 0.9k_c$ to $\hat{k} = 0.55k_c$) toward the center of the spectrum. Moreover, the global Fourier spectrum loses its powdered ring shape [see the inset in the bottom panel of Fig. 4(d)]. In this regime, the spatial profiles

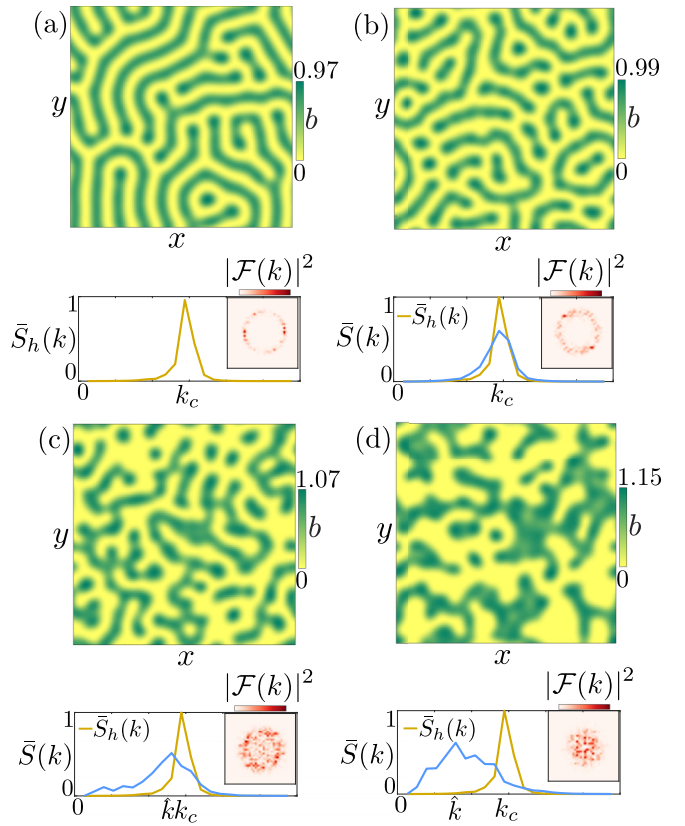


FIG. 4. Spatial characterization of the equilibria from Eq. (2) with $\kappa = 0.6$, $\nu = 0.011$, $\gamma = 0.5$, $\alpha = 0.125$, and $\eta = 0.075$. The top panels in each subfigure display the steady-state vegetated covers from the model equation (2) considering the aridity profiles $\eta(\mathbf{r})$ depicted in Fig. 3, respectively. The blue and yellow curves of the bottom panels indicate the normalized structure factor $\bar{S}(k) \equiv S(k)/S_h(k_c)$, and $\bar{S}_h(k) \equiv S_h(k)/S_h(k_c)$, respectively. $S_h(k)$ is the structure factor in the homogeneous case. The insets in the bottom panels correspond to the Fourier transform $|\mathcal{F}(k)|^2$ of the solutions from Eq. (2). The wavevector \hat{k} illustrates the maximum of $\bar{S}(k)$ when heterogeneities are present.

of the aridity and the biomass density are strongly correlated [see the lower panels of Fig. 3(d) and Fig. 4(d), respectively]. We have termed this spatial structure as *disordered self-organization*.

A phase diagram is generated using numerical simulations of Eq. (2), as shown in Fig. 5(a). The diagram depicts the existence and stability domains of three types of vegetation structures: perfect and imperfect labyrinths and disordered self-organization. We can see that perfect labyrinthine patterns can persist for different combinations of $\sqrt{\Gamma}$ and d/L . Given a minimum intensity level value $\sqrt{\Gamma}$ or degree of correlation d/L , the perfect labyrinths bifurcate to imperfect labyrinthine patterns. When heterogeneities are strong enough, the system exhibits disordered self-organization. We stress that the transition between different labyrinthinelike textures can be triggered solely by $\sqrt{\Gamma}$ or d/L [cf. dashed arrows in Fig. 5(a)]. For example, Fig. 5(b) show the variation of \hat{k}/k_c by fixing $d/L = 0.08$ and moving $\sqrt{\Gamma}$. The insets (i)–(iii) along the diagram illustrate the change in $\bar{S}(k)$ and \hat{k} as the biomass

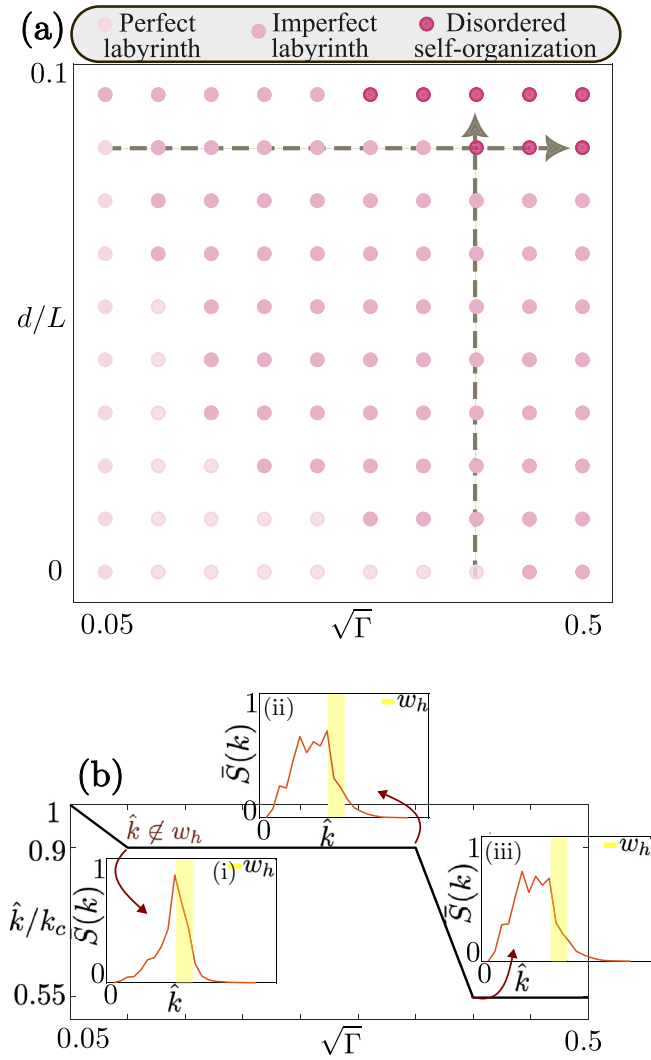


FIG. 5. Phase diagram of vegetation patterns in heterogeneous environments. (a) Phase diagram of the global spatial structure of Eq. (2) with $\kappa = 0.6$, $\nu = 0.011$, $\gamma = 0.5$, $\alpha = 0.125$, and $\eta = 0.075$ as a function of the intensity level $\sqrt{\Gamma}$ and the degree of correlation d/L . The different phases are perfect labyrinthine patterns ($\hat{k} \approx k_c$), imperfect labyrinthine patterns ($\hat{k} \approx 0.9k_c$), and disordered self-organizations ($\hat{k} \approx 0.55k_c$). The dashed gray arrows illustrate possible transition paths between the equilibria. (b) Transition triggered by changing the intensity of the heterogeneities $\sqrt{\Gamma}$ given a correlation $d/L = 0.8$ in the aridity distribution. The insets (i)–(iii) show the normalized structure factor $\bar{S}(k)$ and its peak position \hat{k} . The yellow rectangle depicts the characteristic wavevector range w_h of the labyrinth with $\Gamma = 0$.

departures from the perfect labyrinths. The transition between imperfect labyrinths and disordered self-organization [(ii) \rightarrow (iii)] resembles the disappearance of scurfy labyrinthine patterns in a variational Swift-Hohenberg model [10].

In what follows, we further numerically characterize the labyrinthinelike equilibria using local Fourier transforms. This statistical tool allows us to investigate the self-organization process at small spatial scales. Ideal labyrinthine patterns, for instance, are characterized by their local striped behavior. This feature can be extracted through the averaged

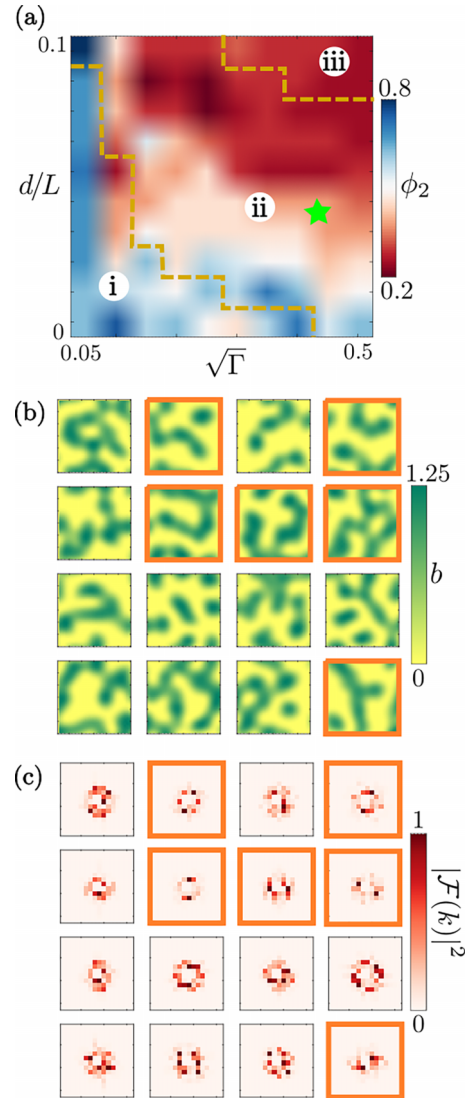


FIG. 6. Phase diagram of the local structure of labyrinthine patterns from Eq. (2) with $\kappa = 0.6$, $\nu = 0.0113$, $\gamma = 0.5$, $\alpha = 0.125$, and $\eta = 0.075$. (a) Colormap of the local two-mode fraction ϕ_2 and correlation d/L of the heterogeneities $\xi(\mathcal{F})$. The segmented yellow lines separate the three regions of Fig. 5: (i) perfect labyrinthine patterns, (ii) imperfect labyrinthine patterns, and (iii) disordered self-organization. (b) Spatial division of a steady-state vegetation pattern, with $\sqrt{\Gamma} = 0.4$ and $d/L = 0.04$ (\star), in windows of size $2.3\lambda_c$. (c) Local Fourier transform $|\mathcal{F}(\vec{k})|^2$ of each window. The orange borders in (b) and (c) indicate that the local pattern fulfills the criteria of being dominantly a stripe.

windowed Fourier transform [10]. The procedure consists of dividing the labyrinthine patterns into N windows of size s , calculating each window's Fourier transform, and then performing a projective average in Fourier space. The result is a single wave mode (stripe) local Fourier spectrum. The critical step is to choose the adequate size s . It has to be small enough to lose the pattern's isotropy and sufficiently big to account for the labyrinth wavelength. Then, the safe choice is $s \approx 2\lambda_c$. Here, we compute the local Fourier transform of the patterns obtained from Eq. (2) in windows of size

TABLE I. Summary of the sensitivity analysis. The sensitivity indices $Si(\phi_2^{pi})$ and $Si(\phi_2^{id})$ are associated to the transition fractions ϕ_2^{pi} and ϕ_2^{id} , respectively.

	η	κ	ν	γ	α	s	th
Original value	0.085	0.6	0.01	0.5	0.125	$2.3\lambda_c$	0.8
$Si(\phi_2^{pi})$	0.10	0.09	0.11	0.07	0.14	0.16	0.26
$Si(\phi_2^{id})$	0.33	0.17	0.12	<0.01	0.23	0.11	0.21

$s = 2.3\lambda_c$ because L/s is an integer number. As a consequence of imperfect labyrinths and disordered self-organizations, the projective average process is not a good approach. To amend this, we introduce the three largest values of the local Fourier transforms $\mathcal{F}_1 \geq \mathcal{F}_2 \geq \mathcal{F}_3$. We define a local window to be dominantly a stripe if $\mathcal{F}_1 = \mathcal{F}_2$ (dominated by two peaks, i.e., a stripe) and $\mathcal{F}_3 \leq 0.8\mathcal{F}_1$. The threshold (th = 0.8), which takes into account the defects of the labyrinths, is selected to maximize the fraction $\phi_2 = N_s/N$ of the labyrinthine pattern under homogeneous conditions. N_s is the number of windows exhibiting stripes.

Figure 6(a) shows the fraction ϕ_2 for different combinations of the intensity level Γ and degree of correlation d/L of the heterogeneities. Additionally, the dashed yellow lines indicate the transitions related to the global spatial structure of the biomass density (see Fig. 5). We note that the transition from perfect labyrinths to imperfect labyrinths is marked by $\phi_2^{pi} = 0.61 \pm 0.06$. As well, imperfect labyrinths become disordered self-organizations when $\phi_2^{id} = 0.30 \pm 0.02$. Figures 6(b) and 6(c) illustrate the local structure and the windowed Fourier transform of an imperfect labyrinthine pattern with $N_s = 6$ as depicted by the orange squares. We note that the transitions in the $(\sqrt{\Gamma}, d/L)$ parameter space depend on the choices of $[\eta, \kappa, \gamma, \alpha, \nu]$. Hence, we highlight that a suitable model parametrization is needed for extending our classifications to natural landscapes.

To test the robustness of our predictions against modeling decisions, we have performed a sensitivity analysis by changing in $\pm 10\%$ the original values of the parameters chosen to observe labyrinths in Eq. (2), the window size s , and the threshold th. When varying the window length, we use the same number of windows N as in the original case by overlapping the windows or by not considering the boundaries of the simulation boxes. To evaluate the sensitivity, the simple sensitivity index $Si(h) = |1 - h_{\min}/h_{\max}|$ is used, where h_{\min} and h_{\max} are a model output when a parameter was decreased or increased, respectively [60]. Values closer to 1 indicate high sensitivity, while $Si(h) < 0.01$ means no sensitivity to variations. We consider the averaged fractions ϕ_2^{pi} and ϕ_2^{id} as model outputs with sensitivity indices $Si(\phi_2^{pi})$ and $Si(\phi_2^{id})$, respectively (see Table I). The transitions from perfect to imperfect labyrinths and imperfect labyrinths to disordered self-organizations are always observed when varying the parameters in Table I.

The sensibility analysis shows that ϕ_2^{id} is sensible to the mean aridity parameter η , which is related to the system being near the boundaries η_l and η_r (see Fig. 2). Additionally, this transition is highly affected by the spatial coupling parameter α and could be related to changes in λ_c . Table I suggests that

both ϕ_2^{pi} and ϕ_2^{id} are sensible to the threshold th, which can be attributed to a wrong counting of the N_s values.

V. DISCUSSION AND CONCLUSIONS

We have investigated the effect of heterogeneous conditions on a pattern-forming ecological model of semiarid and arid landscapes. We have considered a well-known model based on the relationship between the vegetation biomass and the facilitation-competition interactions operating within plants. We have further simplified the analysis by focusing on a reduced model, Eq. (2), and we have restricted our study to a single species that accounts for most of the biomass. Motivated by topographic variations along labyrinthine-like self-organization in Niger and Sudan, we have modeled the heterogeneities as a spatial-dependent aridity parameter. The spatial fluctuations act around a mean aridity value with a certain intensity level. These variations can be correlated with a given correlation length.

By increasing the intensity level and the correlation length of the aridity heterogeneities, we have shown evidence of imperfect labyrinthine patterns and disordered self-organizations. These equilibria of Eq. (2) qualitatively resemble the real labyrinthine-like vegetation patterns observed in satellite images of arid and semiarid landscapes. Furthermore, we have found that perfect labyrinthine patterns are persistent until a critical degree of heterogeneity is reached, where they become imperfect labyrinths. Further increasing the heterogeneities, the spatial structure of the imperfect labyrinth is eventually lost to a disordered self-organization, which is governed by the spatial distribution of the aridity. Based on the peak's position and width of the global structure factor, we have characterized the transitions between equilibria and built a phase diagram. A windowed Fourier transform is used to measure the departure from perfect labyrinthine patterns as a function of heterogeneities.

An interesting future research is the identification of perfect labyrinths, imperfect labyrinths, and disordered self-organizations in real ecosystems by applying the tools and modeling introduced here. To achieve this natural classification, on-site measurements in arid environments populated by labyrinthine-like vegetation patterns will be needed to validate the application of the reduced model, Eq. (2), and to verify if the model parameters are realistic or not. It will be crucial to determine the parameters η and α , as they significantly impact the transitions between labyrinthine-like vegetation patterns. For example, if the labyrinthine-like landscapes of Niger and Sudan (Fig. 1) are well described by model equation (2) and the parameters chosen are characteristic of these particular places, our classification could be applied by extending the local analysis presented here. In fact, our modeling can be used to identify the threshold th for the Sudan and Niger regions in Fig. 1. We hypothesize that these labyrinths are imperfect; that is, they are sustained by a minimum level of spatially correlated heterogeneity, and are the consequence of a combination of a symmetry-breaking instability and heterogeneous environmental conditions. Moreover, *in situ* observations of topography and resource distribution could reveal if a more complex way to incorporate heterogeneities

is needed or if our straightforward approach, based on the intensity level and degree of correlation, is sufficient and reasonable.

Our theoretical findings can be used with other modeling approaches to obtain more realistic labyrinthine patterns, such as reaction-diffusion systems where water dynamics is included explicitly [20,21]. Additionally, our classification can also be applied in different scientific contexts where labyrinths are experimentally observed. For example in fluid mechanics, liquid crystals, optics, biology, and chemistry [61–65], where the sources of heterogeneity are diverse (e.g., thermal fluctuations, experimental imperfections, boundary conditions, inhomogeneous forcing, material defects).

ACKNOWLEDGMENTS

The authors thank two anonymous referees whose constructive comments improve the presentation of this article. S.E.-A. acknowledges the financial support of ANID by Beca Doctorado Nacional 2020-21201376. D.P.-R. acknowledges the financial support of ANID National Ph.D. scholarship 2020-21201484. M.G.C. acknowledges the financial support of ANID–Millennium Science Initiative Program–ICN17_012 (MIRO) and FONDECYT Project No. 1210353. M.T. acknowledges support as a Research Director with the Fonds de la Recherche Scientifique FRS-FNRS, Belgium. We also acknowledge Wallonie-Bruxelles International (WBI).

-
- [1] G. Nicolis and I. Prigogine, *Self-Organization in Non-Equilibrium Systems* (Wiley, New York, 1977).
- [2] M. Cross and H. Greenside, *Pattern Formation and Dynamics in Non-Equilibrium Systems* (Cambridge University Press, New York, 2009).
- [3] J. D. Murray, *Mathematical Biology: I. An Introduction* (Springer, New York, 2002).
- [4] R. V. Solé and J. Bascompte, *Self-Organization in Complex Ecosystems. (MPB-42)* (Princeton University Press, Princeton, NJ, 2006).
- [5] A. M. Turing, The chemical basis of morphogenesis, *Philos. Trans. R. Soc. London, Ser. B* **237**, 37 (1952).
- [6] I. Prigogine and R. Lefever, Symmetry breaking instabilities in dissipative systems. II, *J. Chem. Phys.* **48**, 1695 (1968).
- [7] R. Hoyle and R. B. Hoyle, *Pattern Formation: An Introduction to Methods* (Cambridge University Press, Cambridge, UK, 2006).
- [8] T. Passot and A. C. Newell, Towards a universal theory for natural patterns, *Phys. D (Amsterdam, Neth.)* **74**, 301 (1994).
- [9] M. Le Berre, E. Ressayre, A. Tallet, Y. Pomeau, and L. Di Menza, Example of a chaotic crystal: The labyrinth, *Phys. Rev. E* **66**, 026203 (2002).
- [10] S. Echeverría-Alar and M. G. Clerc, Labyrinthine patterns transitions, *Phys. Rev. Res.* **2**, 042036(R) (2020).
- [11] R. E. Rosensweig, M. Zahn, and R. Shumovich, Labyrinthine instability in magnetic and dielectric fluids, *J. Magn. Magn. Mater.* **39**, 127 (1983).
- [12] K. J. Lee, W. McCormick, Q. Ouyang, and H. L. Swinney, Pattern formation by interacting chemical fronts, *Science* **261**, 192 (1993).
- [13] P. Oswald and P. Pieranski, *Nematic and Cholesteric Liquid Crystals: Concepts and Physical Properties Illustrated by Experiments* (CRC, Boca Raton, FL, 2005).
- [14] S. Park, Manipulating the sequences of block copolymer patterns on corrugated substrates, *Polymer* **180**, 121726 (2019).
- [15] A. Nakhoul, C. Maurice, M. Agoyan, A. Rudenko, F. Garrelie, F. Pigeon, and J.-P. Colombier, Self-organization regimes induced by ultrafast laser on surfaces in the tens of nanometer scales, *Nanomaterials* **11**, 1020 (2021).
- [16] P. Kavle, J. A. Zorn, A. Dasgupta, B. Wang, M. Ramesh, L.-Q. Chen, and L. W. Martin, Strain-driven mixed-phase domain architectures and topological transitions in $\text{Pb}_{1-x}\text{Sr}_x\text{TiO}_3$ thin films, *Adv. Mater.* **34**, 2203469 (2022).
- [17] W. Macfadyen, Soil and vegetation in British Somaliland, *Nature (London)* **165**, 121 (1950).
- [18] R. Lefever and O. Lejeune, On the origin of tiger bush, *Bull. Math. Biol.* **59**, 263 (1997).
- [19] O. Lejeune and M. Tlidi, A model for the explanation of tiger bush vegetation stripes, *J. Veg. Sci.* **10**, 201 (1999).
- [20] J. von Hardenberg, E. Meron, M. Shachak, and Y. Zarmi, Diversity of Vegetation Patterns and Desertification, *Phys. Rev. Lett.* **87**, 198101 (2001).
- [21] M. Rietkerk, M. C. Boerlijst, F. van Langevelde, R. HilleRisLambers, J. v. de Koppel, L. Kumar, H. H. Prins, and A. M. de Roos, Self-organization of vegetation in arid ecosystems, *Am. Nat.* **160**, 524 (2002).
- [22] V. Deblauwe, N. Barbier, P. Couteron, O. Lejeune, and J. Bogaert, The global biogeography of semi-arid periodic vegetation patterns, *Global Ecol. Biogeogr.* **17**, 715 (2008).
- [23] F. Borgogno, P. D’Odorico, F. Laio, and L. Ridolfi, Mathematical models of vegetation pattern formation in ecohydrology, *Rev. Geophys.* **47**, RG1005 (2009).
- [24] V. Deblauwe, P. Couteron, O. Lejeune, J. Bogaert, and N. Barbier, Environmental modulation of self-organized periodic vegetation patterns in Sudan, *Ecography* **34**, 990 (2011).
- [25] L. Mander, S. C. Dekker, M. Li, W. Mio, S. W. Punyasena, and T. M. Lenton, A morphometric analysis of vegetation patterns in dryland ecosystems, *R. Soc. Open Sci.* **4**, 160443 (2017).
- [26] O. Lejeune, M. Tlidi, and P. Couteron, Localized vegetation patches: A self-organized response to resource scarcity, *Phys. Rev. E* **66**, 010901(R) (2002).
- [27] M. Rietkerk, S. C. Dekker, P. C. De Ruiter, and J. van de Koppel, Self-organized patchiness and catastrophic shifts in ecosystems, *Science* **305**, 1926 (2004).
- [28] E. Meron, H. Yizhaq, and E. Gilad, Localized structures in dryland vegetation: Forms and functions, *Chaos* **17**, 037109 (2007).
- [29] P. Couteron, F. Anthelme, M. Clerc, D. Escaff, C. Fernandez-Oto, and M. Tlidi, Plant clonal morphologies and spatial patterns as self-organized responses to resource-limited environments, *Philos. Trans. R. Soc. A* **372**, 20140102 (2014).
- [30] M. Tlidi, E. Berríos-Caro, D. Pinto-Ramo, A. Vladimirov, and M. G. Clerc, Interaction between vegetation patches and gaps: A self-organized response to water scarcity, *Phys. D (Amsterdam, Neth.)* **414**, 132708 (2020).

- [31] M. G. Clerc, S. Echeverría-Alar, and M. Tlidi, Localised labyrinthine patterns in ecosystems, *Sci. Rep.* **11**, 18331 (2021).
- [32] M. Van Rooyen, G. Theron, N. Van Rooyen, W. Jankowitz, and W. Matthews, Mysterious circles in the Namib desert: Review of hypotheses on their origin, *J. Arid. Environ.* **57**, 467 (2004).
- [33] M. Tlidi, R. Lefever, and A. Vladimirov, On vegetation clustering, localized bare soil spots and fairy circles, *Lect. Notes Phys.* **751**, 381 (2008).
- [34] N. Juergens, The biological underpinnings of Namib desert fairy circles, *Science* **339**, 1618 (2013).
- [35] M. D. Cramer and N. N. Barger, Are Namibian “fairy circles” the consequence of self-organizing spatial vegetation patterning? *PLoS One* **8**, e70876 (2013).
- [36] C. Fernandez-Oto, M. Tlidi, D. Escaff, and M. Clerc, Strong interaction between plants induces circular barren patches: Fairy circles, *Philos. Trans. R. Soc. A* **372**, 20140009 (2014).
- [37] D. Escaff, C. Fernandez-Oto, M. G. Clerc, and M. Tlidi, Localized vegetation patterns, fairy circles, and localized patches in arid landscapes, *Phys. Rev. E* **91**, 022924 (2015).
- [38] S. Getzin, K. Wiegand, T. Wiegand, H. Yizhaq, J. von Hardenberg, and E. Meron, Adopting a spatially explicit perspective to study the mysterious fairy circles of Namibia, *Ecography* **38**, 1 (2015).
- [39] C. E. Tarnita, J. A. Bonachela, E. Sheffer, J. A. Guyton, T. C. Coverdale, R. A. Long, and R. M. Pringle, A theoretical foundation for multi-scale regular vegetation patterns, *Nature (London)* **541**, 398 (2017).
- [40] I. Bordeu, M. G. Clerc, P. Couteron, R. Lefever, and M. Tlidi, Self-replication of localized vegetation patches in scarce environments, *Sci. Rep.* **6**, 33703 (2016).
- [41] M. Tlidi, I. Bordeu, M. G. Clerc, and D. Escaff, Extended patchy ecosystems may increase their total biomass through self-replication, *Ecol. Indic.* **94**, 534 (2018).
- [42] M. Tlidi, M. Clerc, D. Escaff, P. Couteron, M. Messaoudi, M. Khaffou, and A. Makhoute, Observation and modelling of vegetation spirals and arcs in isotropic environmental conditions: Dissipative structures in arid landscapes, *Philos. Trans. R. Soc. A* **376**, 20180026 (2018).
- [43] S. Kéfi, M. Rietkerk, C. L. Alados, Y. Pueyo, V. P. Papanastasis, A. ElAich, and P. C. De Ruiter, Spatial vegetation patterns and imminent desertification in Mediterranean arid ecosystems, *Nature (London)* **449**, 213 (2007).
- [44] F. Meloni, G. M. Nakamura, C. R. Granzotti, and A. S. Martinez, Vegetation cover reveals the phase diagram of patch patterns in drylands, *Phys. A (Amsterdam, Neth.)* **534**, 122048 (2019).
- [45] P. Adler, D. Raff, and W. Lauenroth, The effect of grazing on the spatial heterogeneity of vegetation, *Oecologia* **128**, 465 (2001).
- [46] P. D’Odorico, F. Laio, and L. Ridolfi, Vegetation patterns induced by random climate fluctuations, *Geophys. Res. Lett.* **33**, L19404 (2006).
- [47] P. D’Odorico, F. Laio, A. Porporato, L. Ridolfi, and N. Barbier, Noise-induced vegetation patterns in fire-prone savannas, *J. Geophys. Res.* **112**, G02021 (2007).
- [48] T. E. Franz, E. G. King, K. K. Caylor, and D. A. Robinson, Coupling vegetation organization patterns to soil resource heterogeneity in a central Kenyan dryland using geophysical imagery, *Water Resour. Res.* **47**, W07531 (2011).
- [49] I. Rodriguez-Iturbe, Z. Chen, A. C. Staver, and S. A. Levin, Tree clusters in savannas result from islands of soil moisture, *Proc. Natl. Acad. Sci. USA* **116**, 6679 (2019).
- [50] K. Pal, S. Deb, and P. S. Dutta, Tipping points in spatial ecosystems driven by short-range correlated noise, *Phys. Rev. E* **106**, 054412 (2022).
- [51] P. Villa Martín, J. A. Bonachela, S. A. Levin, and M. A. Muñoz, Eluding catastrophic shifts, *Proc. Natl. Acad. Sci. USA* **112**, E1828 (2015).
- [52] M. Scheffer, S. Carpenter, J. A. Foley, C. Folke, and B. Walker, Catastrophic shifts in ecosystems, *Nature (London)* **413**, 591 (2001).
- [53] J. Greenwood, The development of vegetation patterns in Somaliland protectorate, *Geogr. J.* **123**, 465 (1957).
- [54] C. Montana, The colonization of bare areas in two-phase mosaics of an arid ecosystem, *J. Ecol.* **80**, 315 (1992).
- [55] B. Bookhagen and D. W. Burbank, Topography, relief, and TRMM-derived rainfall variations along the Himalaya, *Geophys. Res. Lett.* **33**, L08405 (2006).
- [56] O. Lejeune, M. Tlidi, and R. Lefever, Vegetation spots and stripes: Dissipative structures in arid landscapes, *Int. J. Quantum Chem.* **98**, 261 (2004).
- [57] D. Pinto-Ramos, S. Echeverría-Alar, M. G. Clerc, and M. Tlidi, Vegetation covers phase separation in inhomogeneous environments, *Chaos, Solitons & Fractals* **163**, 112518 (2022).
- [58] M. C. Cross and D. I. Meiron, Domain Coarsening in Systems Far from Equilibrium, *Phys. Rev. Lett.* **75**, 2152 (1995).
- [59] T. Galla and E. Moro, Defect formation in the Swift-Hohenberg equation, *Phys. Rev. E* **67**, 035101(R) (2003).
- [60] S. Echeverría, M. B. Hausner, N. Bambach, S. Vicuña, and F. Suárez, Modeling present and future ice covers in two antarctic lakes, *J. Glaciol.* **66**, 11 (2020).
- [61] J. Gollub, A. McCarriar, and J. Steinman, Convective pattern evolution and secondary instabilities, *J. Fluid Mech.* **125**, 259 (1982).
- [62] M. Seul and D. Andelman, Domain shapes and patterns: The phenomenology of modulated phases, *Science* **267**, 476 (1995).
- [63] Q.-X. Liu, P. M. J. Herman, W. M. Mooij, J. Huisman, M. Scheffer, H. Olf, and J. van de Koppel, Pattern formation at multiple spatial scales drives the resilience of mussel bed ecosystems, *Nat. Commun.* **5**, 5234 (2014).
- [64] A. Pandey, J. D. Scheel, and J. Schumacher, Turbulent superstructures in Rayleigh-Bénard convection, *Nat. Commun.* **9**, 2118 (2018).
- [65] Y. Soupart and P. Aguilera-Rojas (private communication).